


Engineering silver-zwitterionic composite nanofiber membrane for bacterial fouling resistance

V. Anand Ganesh ¹, Binu Kundukad,¹ Dan Cheng,² Sridhar Radhakrishnan,³ Seeram Ramakrishna,⁴ Krystyn J. Van Vliet^{1,5}

¹BioSystems and Micromechanics IRG, Singapore-MIT Alliance for Research and Technology, Singapore 138602

²Center for Environmental Sensing and Modeling IRG, Singapore-MIT Alliance for Research and Technology, Singapore 138602

³Cancer Science Institute of Singapore and Department of Pharmacy, National University of Singapore, Singapore 117599

⁴Department of Mechanical Engineering, Centre for Nanofibers and Nanotechnology, National University of Singapore, Singapore 117575

⁵Department of Materials Science and Engineering, Massachusetts Institute of Technology, Cambridge, Massachusetts 02139

Correspondence to: K. J. Van Vliet (E-mail: krystyn@mit.edu)

ABSTRACT: Bacterial attachment and fouling compromise material performance in applications ranging from marine equipment and bio-medical devices to water treatment systems. For membrane-based water treatment systems, bacterial attachment and biofilm formation decrease water purification efficiency and reduces mechanical durability of the membranes. In this work, we present a concurrent electrospinning and copolymerization approach to engineer composite nanofiber membranes comprising of silver nanoparticle containing poly(vinylidene fluoride-co-hexafluoropropylene) (PVDF-HFP-Ag) nanofibers and [copolymerized zwitterionic sulfobetaine methacrylate-methacryl polyhedral oligomeric silsesquioxane]-poly(methyl methacrylate) nanofibers. We characterized the surface morphology, topography, material chemistry, and wettability of the nanofiber membranes with scanning electron microscopy, atomic force microscopy, Fourier transform infrared spectroscopy, and contact angle measurements. We then challenged these nonwoven membranes with two model microbes, Gram-negative *Pseudomonas aeruginosa* and Gram-positive *Staphylococcus aureus*, and found that the silver-zwitterionic composite nanofiber membrane exhibited superior bacterial fouling resistance by reducing >90% of bacterial attachment when compared to neat PVDF-HFP and PVDF-HFP-Ag nanofiber membranes. This study demonstrates that concurrent electrospinning enables free-standing nanofiber membranes with sustained bacterial fouling resistance, with potential in applications in filtration and water treatment technologies for which antifouling strategies are imperative. © 2019 Wiley Periodicals, Inc. *J. Appl. Polym. Sci.* **2019**, *136*, 47580.

KEYWORDS: bacterial antifouling; concurrent electrospinning; copolymerization; zwitterion

Received 30 May 2018; accepted 13 January 2019

DOI: [10.1002/app.47580](https://doi.org/10.1002/app.47580)

INTRODUCTION

Electrospinning is a versatile technique to engineer metal oxide/polymer nanofibers and other anisotropic nanostructures. This technique can produce fibers with diameter in the range of tens of nanometers to few hundred micrometers by employing a facile approach comprising high-voltage power supply, spinneret containing polymeric solution, and a collector. When a pertinent high voltage is applied, an electrostatically driven polymer jet is ejected from the polymer solution which undergoes bending instability wherein the solvent evaporates resulting in the formation of micro/nanoscale diameter fibers.^{1,2} Nonwoven fiber membranes engineered via electrospinning exhibit high surface to volume ratio, tunable porosity, interconnectivity, microscale interstitial spacing, and malleability to conform to different sizes and shapes.^{3,4} Because of these

advantages, electrospun nanofiber membranes have gained immense attention in applications ranging from tissue engineering, sensors, wearable electronics, and—as is of particular interest herein—membrane based water treatment technologies.^{5–8}

Fluoropolymers such as polyvinylidene fluoride (PVDF) and its derivatives [poly(vinylidene fluoride-co-hexafluoropropylene), PVDF-HFP] are widely used to fabricate nanofiber membranes for water treatment applications, due to the exceptional relative mechanical strength, thermal stability, and chemical resistance of these materials.^{9,10} Despite such advantages, these nanofiber membranes are vulnerable to bacterial colonization because of the high porosity and surface roughness, resulting in the formation of enduring biofilms. Biofilm accumulation, including bacteria and the extracellular polymeric substance they produce, establishes biofouling which

Additional Supporting Information may be found in the online version of this article.

© 2019 Wiley Periodicals, Inc.

deteriorates the water permeability and performance efficiency of membrane-based water treatment systems.^{11–14} Thus, several approaches have been explored to engineer bacterial fouling resistant fluoropolymer nanofibers for water treatment applications. One common approach is to incorporate bactericidal agents such as silver nanoparticles (AgNPs) within or on the nanofibers. AgNPs have shown effective bactericidal activities against broad spectrum of bacteria, attributed to silver ions causing damage to the bacterial cell membrane and also by suppressing the activity of membranous enzymes.^{15,16} However, it is challenging to anchor AgNPs firmly in the nanofiber matrix by physical blending. This is because the Ag^+ ions dissociate from the nanofiber matrix in aqueous environments, and thus the nanofibers lose this antibacterial capacity within ~48 h of exposure.^{17–19}

An alternative approach to bacterial adhesion resistance is to engineer nanofiber surfaces with hydrophilic modifiers such as poly(ethylene glycol), poly(vinyl alcohol), and zwitterionic molecules.^{20–24} Among these, zwitterions containing the pendant groups of phosphobetaine, sulfobetaine, and carboxybetaine have emerged as a promising class of materials for use in the new generation of bacterial anti-adhesion surfaces, as their performance is comparable to and in some cases better than the other hydrophilic modifiers for resisting bacterial adhesion.²⁵ While the mechanism is not understood fully, the charge neutral zwitterionic moieties attract more water molecules, resulting in a high degree of hydration on the surface which is correlated with reduced bacterial adhesion.^{26–28} Among the different zwitterionic monomers, sulfobetaine methacrylate (SBMA) is advantageous for its capacity to polymerize and copolymerize with greater ease than other zwitterions.^{29,30} Various surface modification techniques such as chemical, plasma, irradiation, and flame treatments have been proposed to design fluoropolymer surfaces with SBMA functional groups for bacterial fouling resistance.^{31,32} However, it is challenging to control the surface grafting of highly polar SBMA moieties onto the hydrophobic and chemically inert surface of the randomly oriented fluoropolymer nanofibers.

To leverage the potential of both bactericidal and bacterial anti-adhesion strategies to limit membrane biofouling, we sought to incorporate two nanofiber types within a single nonwoven membrane. This approach required that we also address the aforementioned design challenges of AgNP anchoring in PVDF-HFP nanofibers and impregnation of SBMA moieties within polymeric structures designed for sustained aqueous exposure. Here, we demonstrate this dual functionality by employing concurrent electrospinning and copolymerization approach to engineer novel silver-zwitterionic composite membranes. These nonwoven membranes comprised two different nanofiber types, PVDF-HFP-Ag and [(copolymerized zwitterionic SBMA-MPOSS)-PMMA], randomly entangled with one another to form a unique hybrid nanofiber membrane conferring bacterial fouling resistance. Copolymerization of zwitterionic SBMA with methacryl polyhedral oligomeric silsesquioxane (MPOSS), an organic compound that is nonvolatile and considered environmentally benign,³³ was enabled by this highly symmetric molecules' unique physical, chemical, and mechanical properties.³⁴ The presence of poly(methyl methacrylate) (PMMA) improves the electrospinnability and also facilitates the formation of uniform fibers.³⁵ The resulting nanocomposites exhibited greater processability, hydrolytic stability, and mechanical/chemical

integrity upon wetting.^{36,37} Moreover, we evaluated the surface topography, chemistry, and wettability of these composite membranes, and investigated the bacterial fouling resistance of the membranes. We found that these membranes reduced bacterial adhesion by as much as 90% over 5 days of exposure to Gram-positive and Gram-negative bacterial strains, as compared with widely used fluoropolymer nanofiber membranes, owing to the unique integrated physical and chemical properties of this zwitterionic polymer composite membrane design.

EXPERIMENTAL METHODS

Materials

PVDF-HFP ($M_w = 400\,000$), PMMA ($M_w = 350\,000$), [2-(methacryloyloxy)ethyl]dimethyl-(3-sulfopropyl) ammonium hydroxide (SBMA, 97%, $M_w = 279.35$), 2,2'-Azobis(2-methylpropionitrile) (AIBN, 98%), and silver nitrate (AgNO_3 , 99%) were purchased from Sigma-Aldrich (Singapore). Methacryl POSS cage mixture (formula weight = 1433.97 g/mol) was purchased from Hybrid Plastics, Inc. (Hattiesburg, Mississippi, USA). *N,N*-dimethylformamide (DMF, 99.8%), hexafluoroisopropanol (HFIP, 99%), deionized water, ethanol, phosphate buffered saline (PBS), and Luria-Bertani broth (LB) were obtained from Sigma-Aldrich (Singapore) and were used without any further purification.

Sol-Gel Preparation

Three different homogenous sol-gel solutions were prepared as follows. Pure PVDF-HFP solution was prepared by dissolving 20 wt % of PVDF-HFP in DMF. PVDF-HFP solution with AgNPs was prepared by adding 5 wt % AgNO_3 (with respect to the polymer concentration) in PVDF-HFP/DMF mixture. The solution was heated at 70 °C and placed under magnetic stirring to observe a color change (light brown) indicating the chemical reduction of AgNO_3 to AgNPs by DMF. Zwitterionic SBMA-MPOSS-PMMA solution was prepared by dissolving equal amount (6 wt %) of PMMA/SBMA with 5 wt % of MPOSS and 0.2 wt % of AIBN in HFIP. PMMA was added to improve the electrospinnability (spray to spin transition) of SBMA-MPOSS mixture and also to enhance the formation of uniform and smooth nanofibers.^{38–40} The homogenous mixture was then purged with nitrogen for 15 min and subjected to concurrent electrospinning.

Fabrication of Neat PVDF-HFP Nanofiber Membrane

Neat PVDF-HFP nanofiber membrane was fabricated as follows. The prepared PVDF-HFP solution was loaded into a 10 mL syringe and electrospun using a standard electrospinning machine (NaBond TL-01). The applied voltage and flow rate were set to 20 kV and 1 mL h⁻¹, respectively. The electrospinning process was carried out at room temperature (25 °C) with relative humidity (RH) between 50% and 60%. The distance between the tip of the needle (22 G) and the collector (rotating drum, 200 rpm) was 15 cm. The as-prepared PVDF-HFP nanofiber membrane was heat-treated at 80 °C for 8 h to remove any residual solvent.

Fabrication of Zwitterionic PVDF-HFP Composite Nanofiber Membrane (ZPC) and Composite Nanofiber Membrane with AgNPs (ZPC-Ag)

Two solutions, PVDF-HFP and zwitterionic SBMA-MPOSS-PMMA, were electrospun concurrently as shown in Figure 1(e) to fabricate ZPC. Both the solutions were loaded in 10 mL syringes

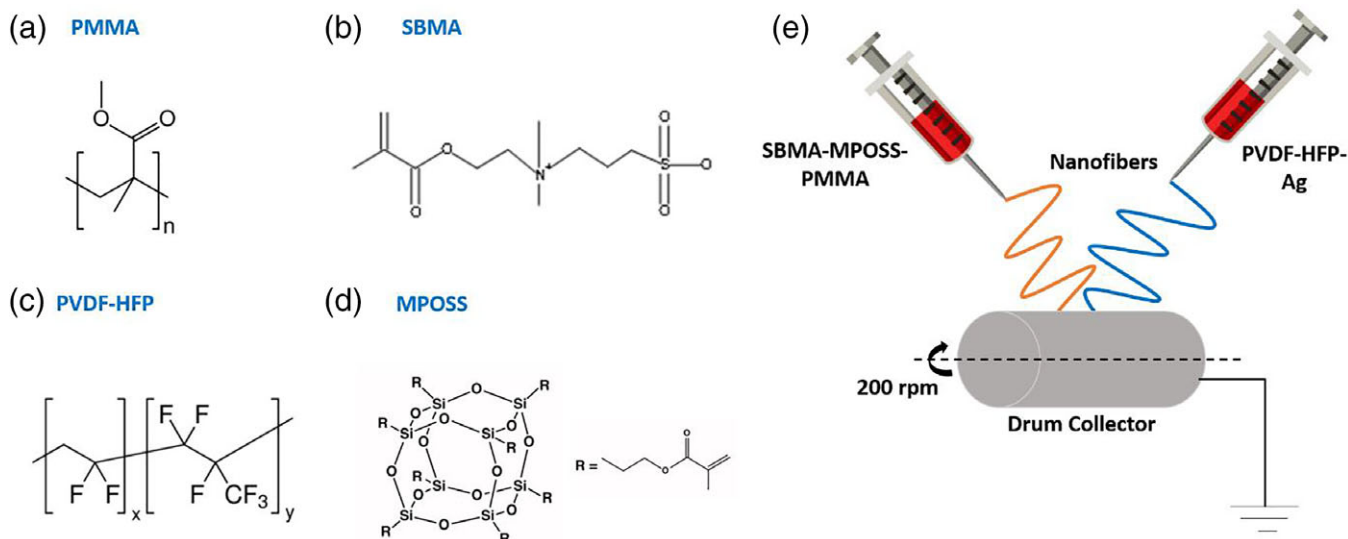


Figure 1. Chemical structure of (a) poly(methyl methacrylate) (PMMA), (b) sulfobetaine methacrylate (SBMA), (c) poly(vinylidene fluoride-*co*-hexafluoro-propylene) (PVDF-HFP), (d) methacryl polyhedral oligomeric silsesquioxane (MPOSS), and (e) schematic representation of the concurrent electrospinning setup. [Color figure can be viewed at wileyonlinelibrary.com]

and electrospun concurrently using 22 G needles with an uniform flow rate of about 1 mL h^{-1} . The applied voltage and spinning distance between the needle tips and drum collector were set at 20 kV

and 15 cm, respectively. The entire process was carried out inside a closed chamber with temperature and RH maintained at $25 \text{ }^\circ\text{C}$ and 50%–60%, respectively. In order to fabricate ZPC-Ag nanofiber

Copolymerization reaction

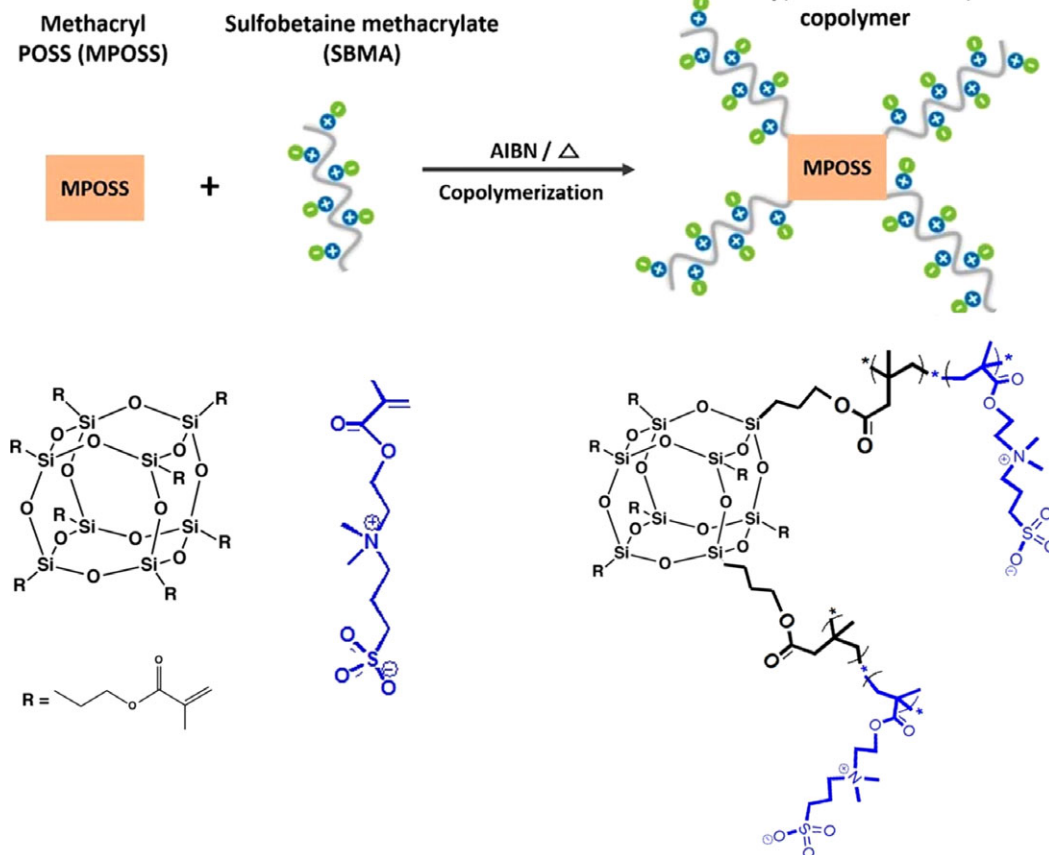


Figure 2. Schematic illustration of the copolymerization reaction between SBMA and MPOSS monomers to form poly(SBMA-*co*-MPOSS) copolymer. [Color figure can be viewed at wileyonlinelibrary.com]

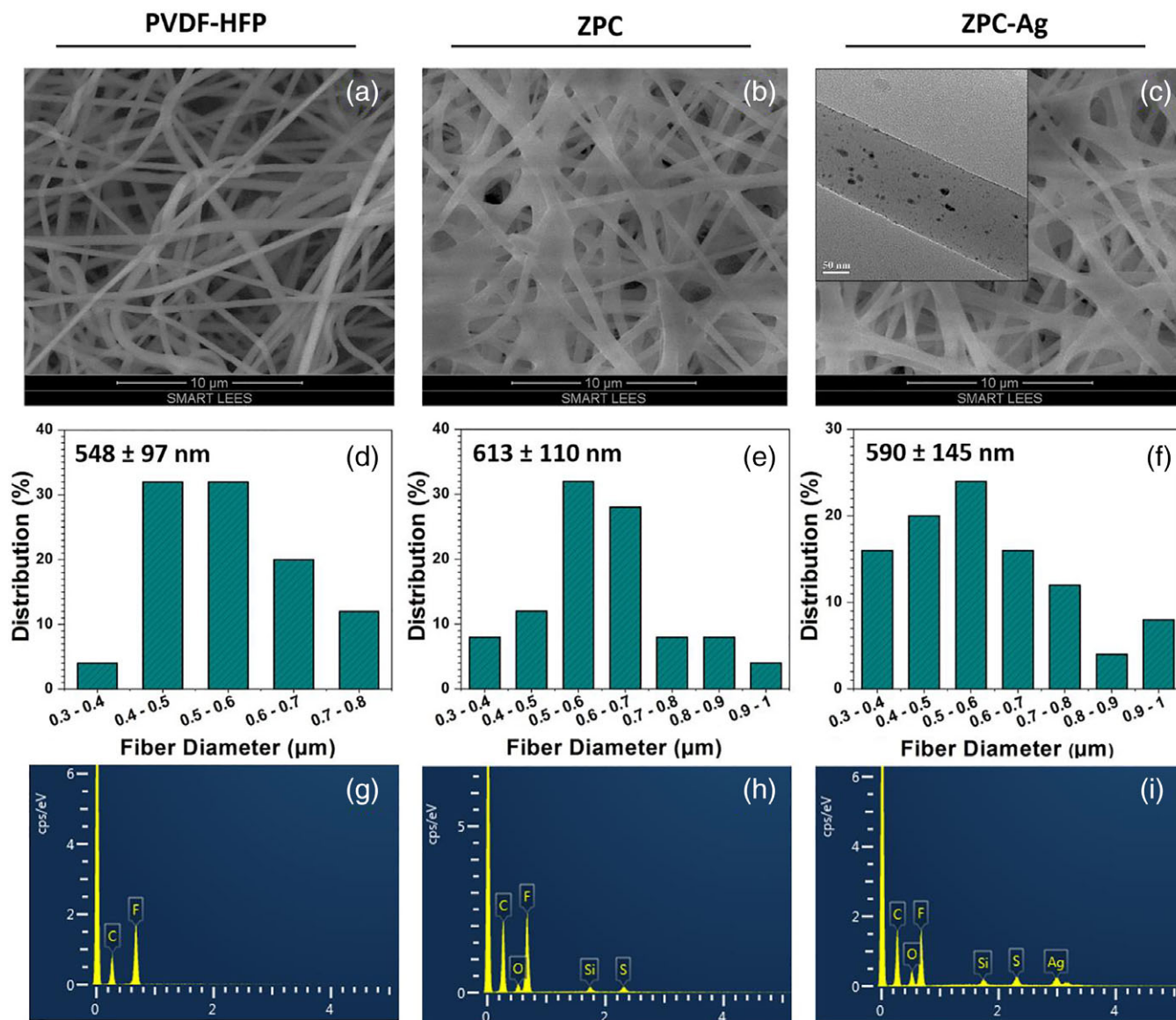


Figure 3. SEM images of the surface morphology of electrospun nanofiber membranes and the fiber diameter distributions. (a, d) PVDF-HFP membrane; (b, e) zwitterionic PVDF-HFP composite membrane (ZPC); (c, f) zwitterionic PVDF-HFP composite membrane with silver nanoparticles (ZPC-Ag) (Inset in c: TEM image showing the presence of silver nanoparticles in ZPC-Ag membrane). EDS spectra of (g) PVDF-HFP membrane, (h) ZPC membrane, and (i) ZPC-Ag membrane. [Color figure can be viewed at wileyonlinelibrary.com]

membrane, pure PVDF-HFP solution was replaced by PVDF-HFP with AgNPs solution. The as-prepared nanofiber membranes (ZPC and ZPC-Ag) were then heat-treated at 65 °C to initiate the free-radical copolymerization reaction between SBMA and MPOSS (Figure 2), between the methacrylate side chains of SBMA and MPOSS monomers.^{41–45} The polymerization was then carried out at elevated temperature (110 °C) in vacuum, resulting in the formation of PVDF-HFP-poly(SBMA-co-MPOSS)-PMMA composite (ZPC) nanofiber membrane. The copolymerized membranes were rinsed with deionized (DI) water to remove the unreacted monomers and then vacuum dried at 80 °C.

Characterization of Nanofiber Membranes

Nanofiber membranes (PVDF-HFP, ZPC, and ZPC-Ag) were coated with a thin layer of gold using a sputter coater before their

morphology was examined using a scanning electron microscopy (SEM). The images were captured using a field-emission SEM instrument (JEOL, JSM-6700F) operated at 5 kV. The same machine was used to obtain the energy dispersive X-ray spectroscopy (EDS). The fiber diameter and distribution were determined by measuring 50 random fibers from five micrographs using *ImageJ* software. The contact angle measurements were carried out using a contact angle measurement setup (VCA optima contact angle equipment from AST Products) in static sessile drop mode at room temperature. The values reported were the averages of at least 10 measurements made on different areas of the nanofiber membranes. Fourier transform infrared (FTIR) spectra were obtained with a Perkin-Elmer spectrometer. Spectra were recorded at a resolution of 4 cm⁻¹ and a total of 64 scans at room temperature. TEM images of the fibers containing the AgNPs were taken

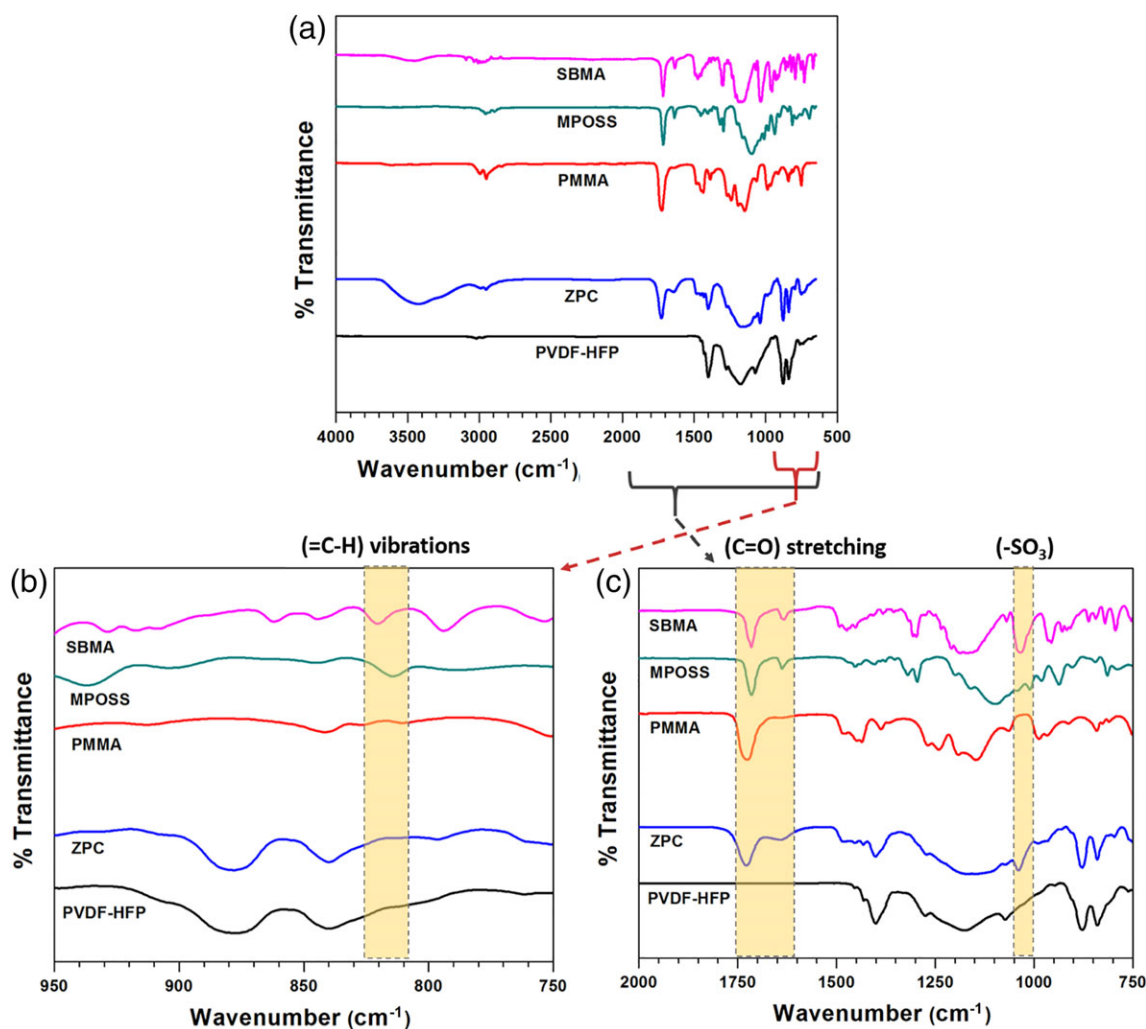


Figure 4. FTIR spectra of SBMA and MPOSS monomers, PMMA polymer, PVDF-HFP membrane, and zwitterionic PVDF-HFP composite (ZPC) membrane. [Color figure can be viewed at wileyonlinelibrary.com]

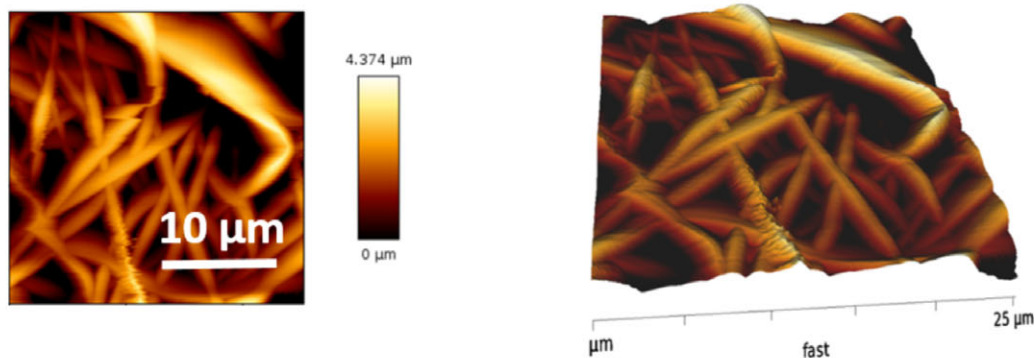
by a high-resolution transmission electron microscope (JEOL 3010 operated at 300 kV). The size of the nanoparticles was measured using *ImageJ*. Atomic force microscopy (AFM) imaging was done at room temperature in air with a Nanowizard II atomic force microscope (JPK Instruments, Berlin, Germany). Images were acquired in the tapping mode with nanosensor silicon (Si) cantilevers (spring constant of 10–130 N/m) and operated below their resonance frequency (typically 200–500 kHz). Surface energy of the membranes were calculated by measuring the contact angle made by DI water and ethylene glycol (as a second probe liquid) using Owens–Wendt and Fowkes method.^{46,47}

Bacterial Fouling Studies on the Nanofiber Membranes

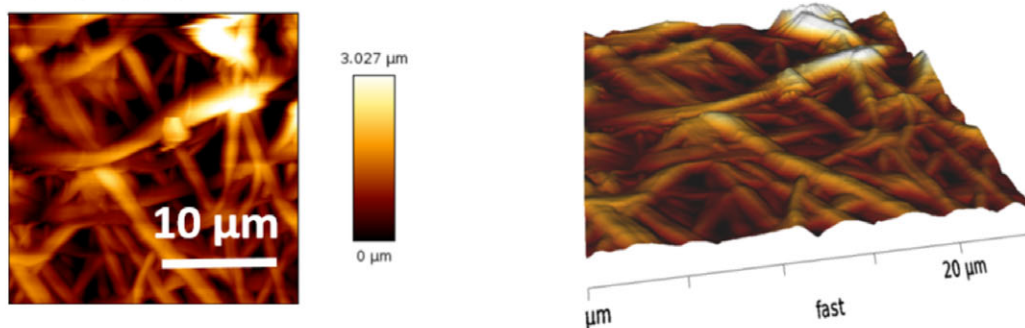
Free standing nanofiber membranes (PVDF-HFP, ZPC, and ZPC-Ag) were cut into squares with a uniform area (4 cm²) and thickness (120–130 μm) and attached at the base of the 6-well plate. The model Gram-positive and Gram-negative micro-organisms, *Staphylococcus aureus*, *Pseudomonas aeruginosa*, respectively, were used for the bacterial fouling studies. Fluorescently tagged strains were constructed by the insertion of a mini-Tn7-enhanced green fluorescent protein-Gmr cassette as described previously.⁴⁸ Overnight

cultures of *S. aureus* and *P. aeruginosa* strains were grown in LB broth at 37 °C under shaking conditions (130 rpm). The bacterial cultures were then diluted to an optical density at 600 nm (OD₆₀₀) of 0.3 and transferred into the six-well plate containing the nanofiber membranes and incubated for 2 h at 25 °C. After facilitating the initial attachment of the bacteria onto the nanofiber membranes, 10% LB medium was supplied every 5 h for a period of 5 days to enable the bacteria to grow and form stable biofilms. Nanofiber membranes with attached bacteria/biofilm were removed from the six-well plate and washed with PBS and DI water to remove loosely adhered bacteria. *P. aeruginosa* and *S. aureus* attachments were evaluated by Bactiquant surface analysis assay (purchased from Mycometer Asia Pte. Ltd., Singapore.) that quantifies the level of bacteria on the surface by measuring the hydrolase activity of the live bacteria using a fluorometer.⁷⁴ Negative control was performed similarly for the clean membrane without any bacterial growth. Significant differences between the nanofiber membrane samples were determined with an unpaired student *t* test. Significance ($P < 0.001$) is denoted in graphs by asterisk (*). Furthermore, the bacterial colony coverage on the nanofiber membranes was monitored using fluorescent imaging performed by

(a) PVDF-HFP Membrane



(b) ZPC Membrane



(c) ZPC-Ag Membrane

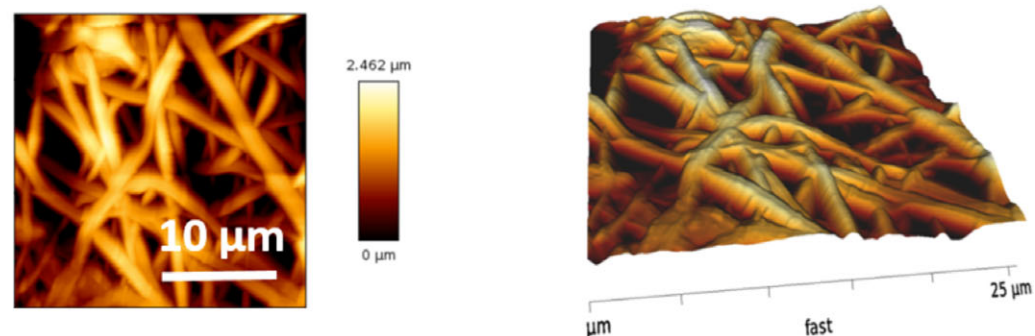


Figure 5. Tapping mode AFM images of (a) PVDF-HFP membrane, (b) ZPC membrane, and (c) ZPC-Ag membrane. The dimensions of the scan images are $25 \mu\text{m} \times 25 \mu\text{m}$. [Color figure can be viewed at wileyonlinelibrary.com]

Olympus FluoView Confocal Microscope (open pin-hole setting) with $20\times$ objective. In order to visualize the bacterial attachment on the nanofiber membranes, the membranes were stained using DiI (1,1'-diiododecyl-3,3,3',3'-tetramethylindocarbocyanine perchlorate) stain. Images were acquired using two image channels, GFP 488 and Alexa 594.

RESULTS AND DISCUSSION

Nanofiber membranes of several distinct polymer compositions were fabricated via electrospinning. Figure 1(a–d) shows the chemical structure of PMMA, SBMA, PVDF-HFP, and MPOSS,

respectively. Figure 1(e) schematizes the concurrent electrospinning setup used to fabricate nanofiber membranes. Neat PVDF-HFP nanofiber membranes were prepared by direct electrospinning of PVDF-HFP solution. The zwitterionic PVDF-HFP composite nanofiber membrane is referred to hereafter as ZPC, or as ZPC-Ag for composites including AgNPs. These membranes were fabricated by concurrent electrospinning of PVDF-HFP (with or without AgNPs in the PVDF-HFP solution) and zwitterionic SBMA-MPOSS-PMMA solutions. ZPC and ZPC-Ag membranes were then heat treated to enable the copolymerization between SBMA and MPOSS (Figure 2). Figure 3(a–f) shows the surface morphology and fiber diameter distribution of PVDF-HFP, ZPC, and ZPC-Ag

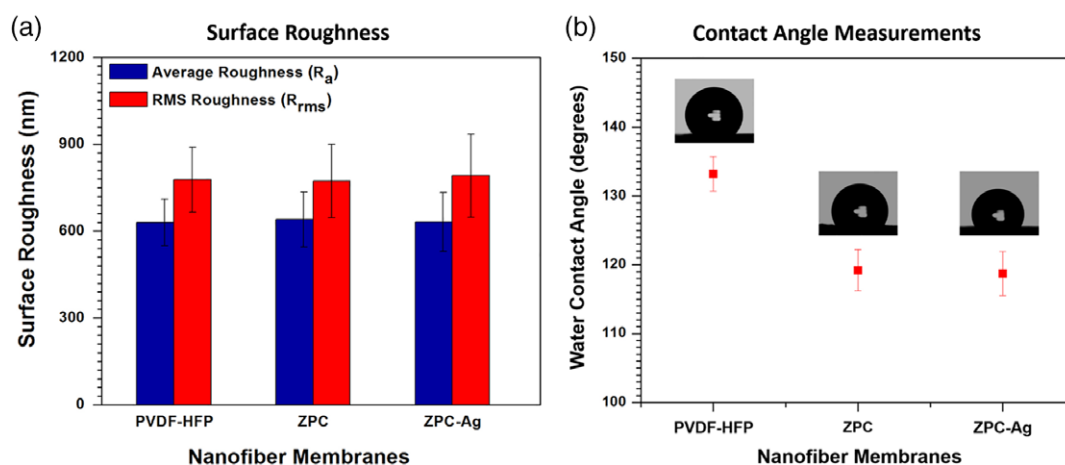
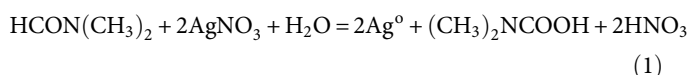


Figure 6. (a) Surface roughness (average roughness R_a , root-mean-square roughness R_{rms}) of PVDF-HFP, ZPC, and ZPC-Ag membranes measured by AFM; (b) static contact angle made by water droplet (5 μ L) on PVDF-HFP, ZPC, and ZPC-Ag membranes. [Color figure can be viewed at wileyonlinelibrary.com]

nanofiber membranes. The membranes comprising PVDF-HFP, ZPC, and ZPC-Ag nanofibers exhibited smooth and apparently defect free morphology. Furthermore, ZPC membranes constituted randomly entangled fiber network made of PVDF-HFP nanofibers and poly(SBMA-co-MPOSS)-PMMA nanofibers [Figures 3(b,c)]. Abrigo *et al.* reported that the diameter of the nanofibers influence the ability of bacterial species to proliferate and colonize the fiber network.⁴⁹ In order to reduce the bacterial proliferation, and to eliminate the effect of fiber geometry on bacterial adhesion across the three different membranes (PVDF-HFP, ZPC, and ZPC-Ag), we fabricated all the membranes with uniform fiber diameter (\sim 600 nm) and thickness (\sim 120–130 μ m) with thickness measured by cross-sectional SEM images (Supporting Information Section 1, Table ST1 and Figure S1).

The inset in Figure 3(c) shows the TEM image of a single PVDF-HFP nanofiber with AgNPs. AgNPs were synthesized by chemical reduction approach as described in eq. (1).⁵⁰



As DMF was the solvent for PVDF-HFP in our system, we synthesized AgNPs *in situ* within the PVDF-HFP solution to fabricate nanofibers embedded with AgNPs without using any external additives.

The average diameter of AgNPs was 10.2 ± 3.8 nm. The elemental composition of the nanofiber membranes were analyzed by EDS (Supporting Information Section 2, Table ST2 and Figure S2). Figure 3(g,h) shows the EDS spectra of both PVDF-HFP and ZPC nanofiber membranes. The spectra of PVDF-HFP membrane showed peaks of carbon and fluorine while the copolymerized ZPC membrane showed additional peaks of sulfur, silicon, and oxygen, indicating the presence of poly(SBMA-co-MPOSS) and PMMA. The additional silver peak in Figure 3(i) confirmed the presence of AgNPs in the ZPC-Ag membrane.

Figure 4 shows the FTIR spectra of SBMA, MPOSS monomers, PMMA polymer, PVDF-HFP, and ZPC nanofiber membranes. The FTIR spectra of all the materials showed the presence of

their respective functional groups. This analysis confirmed the composition of all the functional and support polymers in the ZPC membrane to exhibit their corresponding physicochemical properties. The FTIR spectra of the bare SBMA and MPOSS monomers showed the carbonyl (C=O) stretching at 1709 and at 1715 cm^{-1} , respectively. The ZPC membrane showed the PMMA carbonyl peak as major broad peak at 1715 cm^{-1} masking the peaks from SBMA and MPOSS carbonyls. Both the ZPC membrane and SBMA monomer exhibited (C–N) bond stretching of SBMA at 1640 cm^{-1} . The characteristic symmetric and asymmetric stretching vibrations of sulfonyl group ($-\text{SO}_2$) were observed at 1040 and 1175 cm^{-1} for SBMA monomer while there was a slight shift to 1036 cm^{-1} and to 1157 cm^{-1} in the case of ZPC membrane. The O–Si–O bond of MPOSS monomer was observed at 1100 cm^{-1} and it was slightly shifted to right in the case of the ZPC membrane. Both ZPC membrane and pure PVDF-HFP membrane show the vibrational band of α -phase and β -phase of PVDF-HFP at 850–870 cm^{-1} , respectively. The unsaturated ($-\text{CH}$) stretching vibration of SBMA monomer was observed at 3089 cm^{-1} , while the saturated ($-\text{CH}$) stretching peak of copolymerized ZPC membrane and PMMA were observed around 2920 cm^{-1} and that of PVDF-HFP was seen at 3000 cm^{-1} , respectively. The peaks at 820 cm^{-1} in SBMA and 814 cm^{-1} in MPOSS monomers correspond to the out-of-plane bending vibration of the (C–H) bond in the carbon–carbon double bond. These two peaks did not appear in the ZPC membrane spectrum, implying the disappearance of the carbon–carbon double bond, thus confirming the copolymerization between SBMA and MPOSS monomers to form poly(SBMA-co-MPOSS).⁵¹

To ascertain the copolymerization of the SBMA and MPOSS monomers, we synthesized poly(SBMA-co-MPOSS) copolymer conventionally and compared its FTIR spectra with poly(SBMA-co-MPOSS) formed in the ZPC membrane fabricated by concurrent electrospinning process [Supporting Information Section 3, Figure S3(a)]. FTIR spectrum of conventionally synthesized poly(SBMA-co-MPOSS) copolymer showed the presence of characteristic SBMA and MPOSS peaks to confirm copolymerization [Supporting Information Figure S3(b)]. Similar to the

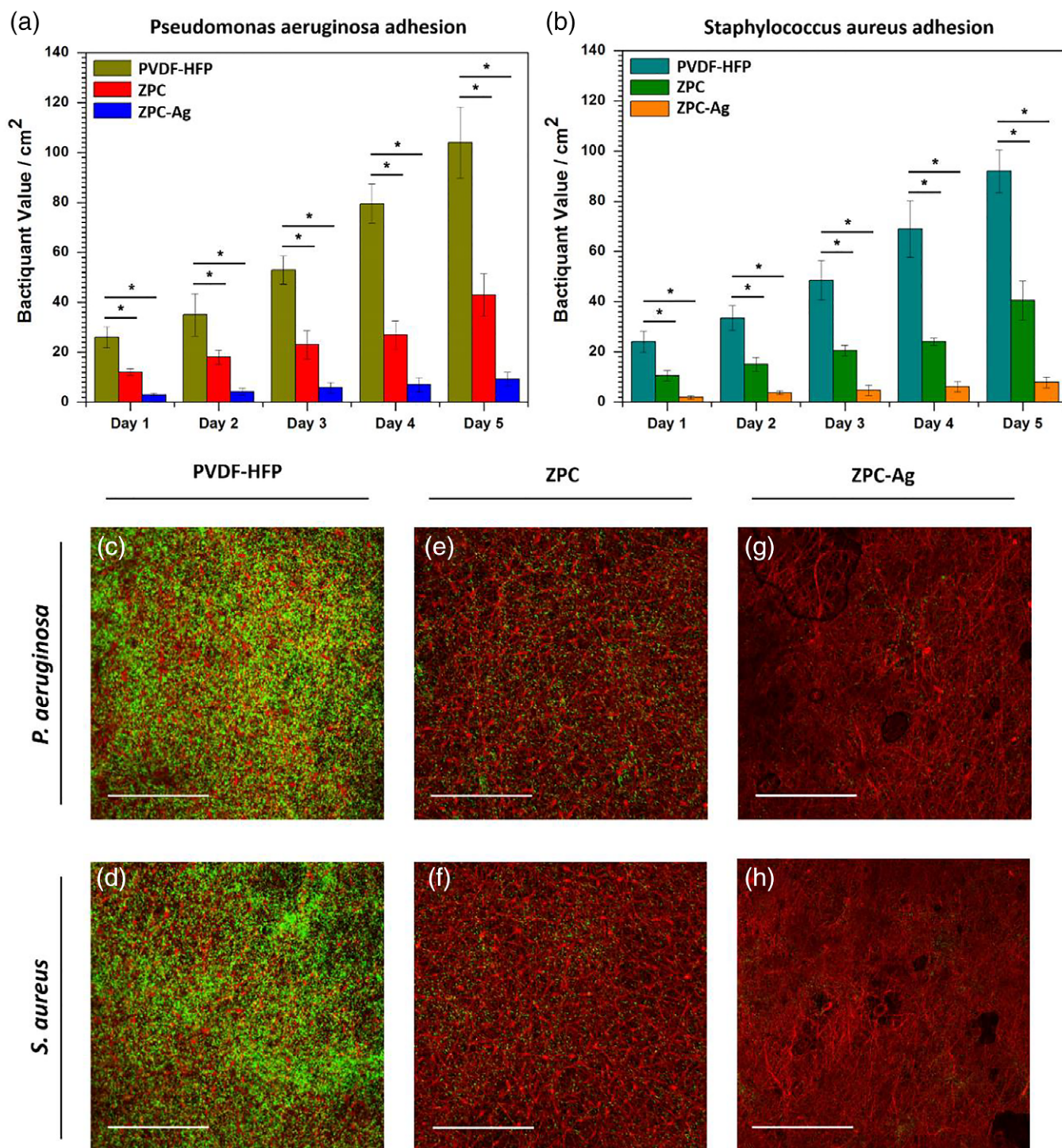


Figure 7. (a, b) *P. aeruginosa* and *S. aureus* adhesion studies on different membranes (PVDF-HFP, ZPC, and ZPC-Ag) for 5 days using Bactiquant surface analysis assay. Error bars denote standard error and one asterisk (*) denotes $P < 0.001$ significance between samples; (c–h) representative confocal microscopy images of PVDF-HFP, ZPC, and ZPC-Ag membranes upon exposure to *P. aeruginosa* or *S. aureus* after day 5 (Scale bar: 100 μm). Fibers (red in color) are stained with DiI fluorescent dye and bacteria (green in color) are tagged with green fluorescent protein (GFP). [Color figure can be viewed at wileyonlinelibrary.com]

nanofiber copolymer illustrated earlier, the (—CH) stretching vibration bands of poly(SBMA-co-MPOSS) were seen shifted right to the saturated (—CH) region [Supporting Information Figure S3(c)]. We also observed the disappearance of out-of-plane bending vibration bands corresponding to carbon–carbon

double bond of monomers, SBMA and MPOSS at 820 and 814 cm^{-1} respectively, which further confirmed the identical copolymerization of the monomers both at conventional synthesis and also in nanofibers form [Supporting Information Figure S3(d)].

For any solid surface, its apparent hydrophobicity is significantly affected by both surface roughness and surface energy of the material.⁵² For an ideal surface (smooth and homogeneous), the surface energy is a measure of the intrinsic surface hydrophobicity determined by the chemical structure and intermolecular forces of the surface. The decrease in surface energy contributes to the increase in hydrophobicity of the surface. However, for real surfaces, both roughness and surface energy contribute to the apparent surface hydrophobicity.⁵³ In order to ensure that the surface topography remains consistent across the three different nanofiber membranes (PVDF-HFP, ZPC, and ZPC-Ag), we engineered the nanofibers with uniform fiber diameter and thickness. The surface topography of the membranes, characterized by AFM, showed that the average (R_a) and root-mean-square (R_{rms}) roughness values are consistent across all the three membranes [Figures 5 and 6(a), Supporting Information Table ST3]. The wettability of the nanofiber membranes was investigated by measuring the static contact angle made by deionized water droplets (droplet volume: 5 μ L) on the membranes. Due to the inherent hydrophobic nature of PVDF-HFP and the nanoscale roughness induced by the nanofiber morphology, PVDF-HFP membranes exhibited a relatively high water contact angle of $\sim 134^\circ$.^{54,55} The ZPC and ZPC-Ag membranes showed lower contact angles ($118 \pm 2^\circ$) than that of pure PVDF-HFP membrane [Figure 6 (b)]. Furthermore, the surface energy of the membranes are determined using Owens–Wendt and Fowkes method by measuring the contact angle made by water and ethylene glycol droplets on the surface of the nanofibers. The surface energy of the membranes (PVDF-HFP, ZPC, and ZPC-Ag) are calculated to be 52.42, 70.85, and 72.05 mN/m, respectively (Supporting Information Section 4, Supporting Information Table ST4). Although the surface topography remains consistent across the three nanofiber membranes, the decrease in water contact angle and increase in surface energy are attributed to the superhydrophilic nature of SBMA moieties present in the poly(SBMA-*co*-MPOSS) copolymer. Zwitterionic SBMA moieties induces electrostatic interactions with water molecules thereby leading to surface hydration, which allows for a reduced water contact angle and increased surface energy.^{56–58} This observation verified the presence of the zwitterionic copolymer in ZPC and ZPC-Ag membranes.

The bacterial antifouling ability of the PVDF-HFP, ZPC, and ZPC-Ag nanofiber membranes was evaluated for up to 5 days exposure, using one of two model bacterial strains, Gram-negative *P. aeruginosa* or Gram-positive *S. aureus*. Figure 7(a,b) shows that pure PVDF-HFP nanofiber membranes exhibited no resistance to bacterial fouling, and thus the intensity of bacterial adhesion increased daily as expected for this control membrane. After 5 days of incubation, the PVDF-HFP membrane was completely colonized by both *P. aeruginosa* and *S. aureus* bacteria [Figure 7(c,d)]. On the contrary, the ZPC membrane reduced the bacterial adhesion by 60% compared to the PVDF-HFP membrane, which is remarkable in fact that the electrospun membranes have the ability to readily adsorb bacteria due to high membrane porosity.^{59,60} The zwitterionic SBMA moieties present in the poly(SBMA-*co*-MPOSS) copolymer increase chain mobility and attract water molecules, which is considered to promote a thermodynamic hydration

barrier which in turn repels bacterial adhesion.^{61,62} As a result, the ZPC membrane exhibited good bacterial anti-adhesion ability against both *P. aeruginosa* and *S. aureus* bacteria, when compared to PVDF-HFP membrane [Figure 7(e,f)].

In order to further enhance the antibacterial ability, AgNPs were introduced into the ZPC nanofiber matrix to fabricate membranes (ZPC-Ag) with dual functionality of both bactericidal and bacterial anti-adhesion properties. The results [Figure 7(g,h)] showed that ZPC-Ag membranes exhibited ultralow bacterial adhesion, with more than 90% reduction of attachment for both *P. aeruginosa* and *S. aureus* bacteria even after 5 days of incubation. This resulted in excellent biofouling resistance (Figure 8). Membranes comprising only PVDF-HFP-Ag nanofibers maintained biofouling resistance for only 2 days (Supporting Information Section 5, Figures S4–S6).

The bacterial adhesion resistance of the ZPC-Ag membrane could be attributed to the randomly entangled [PVDF-HFP-Ag/Poly(SBMA-*co*-MPOSS)-PMMA] nanofiber network, which facilitated the interaction between the carbonyl moieties of PMMA and MPOSS with AgNPs.^{63–66} Furthermore, ionic interactions also exist between the anionic (SO_3^-) groups of poly(SBMA-*co*-MPOSS) and cationic silver ions of AgNPs.^{67–69} These physicochemical interactions likely contribute towards the stabilization/anchoring of the AgNPs in the ZPC-Ag nanofibers thus inhibiting the bacterial adhesion and bacterial fouling over extended durations of exposure.

It is worthwhile to mention that bacterial fouling is caused by the attachment of both live and dead bacteria. Accumulation of dead bacteria on the membrane surface will not only shield the functional groups and decrease the bactericidal efficiency but also serve as a habituation layer to provide nutrients for subsequent bacterial adhesion.^{70,71} Therefore, in addition to the bactericidal property, the membrane must possess the ability to repel the dead bacteria to exhibit an improved and efficient bacterial fouling resistance. In order to study the adhesion of dead bacteria to the ZPC-Ag membrane surface, the ZPC-Ag and PVDF-HFP membrane samples (PVDF-HFP membrane serves as a control) were kept immersed in the *S. aureus* bacterial culture solution for 5 days to facilitate bacterial adhesion and subsequent biofilm formation. The samples were then exposed in UV light for 1 h and also heat treated at 100 $^\circ\text{C}$ for 1 h to ensure that all bacteria attached to the membrane samples are killed. The samples were then washed using PBS and DI water (3 times each) to remove loosely adhered bacteria. Figure S7 (Supporting Information Section 6) shows the typical SEM images of the presence of dead bacteria on the PVDF-HFP and ZPC-Ag membranes. From Supporting Information Figure S7(a), it can be seen that the dead *S. aureus* bacterial cells were deposited on the surface of PVDF-HFP nanofibers, thereby clogging the pores of the membrane and leads to promoting subsequent bacterial adhesion and bacterial fouling. On the contrary, the presence of zwitterionic moieties in the ZPC-Ag nanofiber matrix suppressed the adhesion of bacteria and also facilitated easy removal of the dead bacteria from the membrane surface when subjected to washing with PBS and DI water [Supporting Information Figure S7(b)]. These results confirmed that the ZPC-Ag membrane not only has the ability to kill bacteria but also prohibit the accumulation of dead bacteria on

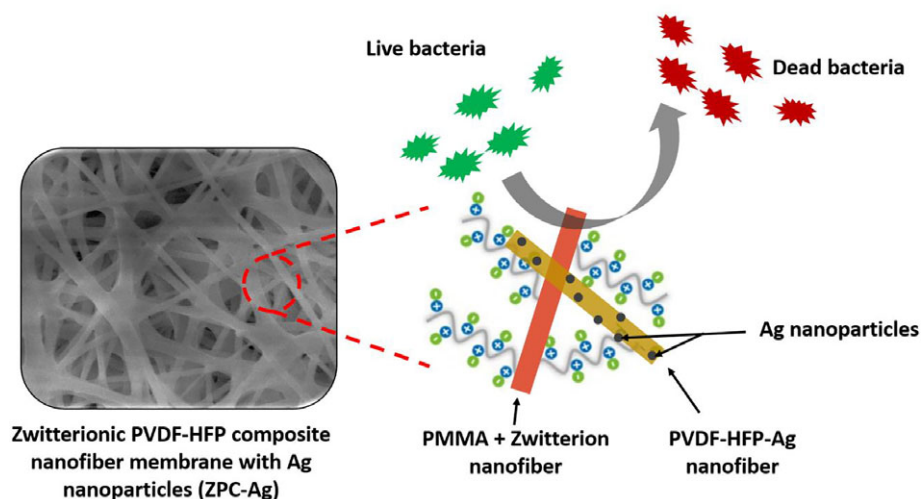


Figure 8. Schematic illustration of bacterial interaction with Zwitterionic PVDF-HFP composite membrane with silver nanoparticles (ZPC-Ag). [Color figure can be viewed at wileyonlinelibrary.com]

the membrane surface thereby exhibiting remarkable bacterial fouling resistance.

We have also evaluated the particulate filtration performance of the ZPC-Ag membrane by using a simple custom made dead-end filtration set up (Supporting Information Section 7, Figure S8). DI water containing polystyrene beads (size: 1.1 μm mean diameter) was made to pass through the membrane by applying a constant pressure of 0.8 bar and water flux is calculated.^{72,73} It is observed that the ZPC-Ag membrane effectively filtered out the polystyrene beads which are seen accumulated on the surface of the nanofibers (Supporting Information Section 7, Figure S9). Furthermore, the ZPC-Ag membrane showed a substantial increase (more than threefold) in the water flux when compared to PVDF-HFP control membrane (Supporting Information Section 7, Figure S10, Videos SV1 and SV2). The decrease in hydrophobicity due to the presence of zwitterionic moieties on the ZPC-Ag membrane resulted in improving the water flux significantly. The high flux, ability to filter out micro-pollutants and exceptional bacterial fouling resistance of the ZPC-Ag membranes make them a promising system for filtration and wastewater treatment applications.

CONCLUSIONS

Here we successfully engineered novel composite nanofiber membranes (zwitterionic polymer composites, or ZPC) with sustained bacterial fouling resistance by concurrent electrospinning of PVDF-HFP and SBMA-MPOSS-PMMA solutions, followed by copolymerization of zwitterionic SBMA with MPOSS. We investigated the ability of the ZPC membranes, with and without *in situ* synthesis of AgNPs in these nanofibers, to inhibit bacterial fouling by exposing the membranes against *S. aureus* and *P. aeruginosa* for 5 days. ZPC membranes reduced colonization by 60%, and by >90% when Ag nanoparticles were synthesized within the nanofibers, by both bacterial species when compared to fluoropolymer nanofiber membranes. The concurrent electrospinning resulted in the formation of a randomly entangled

nanofiber network that assisted in anchoring the AgNPs in the nanofibers matrix through (carbonyl-Ag) and (zwitterionic-Ag) interactions. This silver-zwitterionic polymer composite nanofiber membrane thus limited the bacteria adhesion, and then leveraged the bactericidal action of silver ions against any adherent microbes. Consequently, ZPC-Ag nanofiber membranes exhibited superior bacterial antifouling ability for two bacterial strains when compared to PVDF-HFP, PVDF-HFP-Ag, and ZPC nanofiber membranes, over 5 days of exposure in the absence of shear flow. Such electrospun structures can now be considered for novel membrane based water treatment systems and bio-filters that require biofouling resistance over extended durations of at least days of microbial exposure in aqueous environments.

ACKNOWLEDGMENTS

V.A.G. acknowledges the SMART Scholar Fellowship from the Singapore-MIT Alliance for Research and Technology. This research was supported by the National Research Foundation of Singapore, through the Singapore MIT Alliance for Research and Technology's BioSystems and Micromechanics (BioSyM) IRG research program.

REFERENCES

- Persano, L.; Camposeo, A.; Tekmen, C.; Pisignano, D. *Macromol. Mater. Eng.* **2013**, *298*, 504.
- Shin, Y. M.; Hohman, M. M.; Brenner, M. P.; Rutledge, G. C. *Appl. Phys. Lett.* **2001**, *78*, 1149.
- Deitzel, J.; Kleinmeyer, J.; Harris, D.; Tan, N. B. *Polymer.* **2001**, *42*, 261.
- Zhang, C.; Li, P.; Cao, B. *J. Appl. Polym. Sci.* **2016**, *133*, 43475.
- Murugan, R.; Ramakrishna, S. *Tissue Eng.* **2006**, *12*, 435.
- Kim, I. D.; Rothschild, A.; Lee, B. H.; Kim, D. Y.; Jo, S. M.; Tuller, H. L. *Nano Lett.* **2006**, *6*, 2009.

7. Najafabadi, A. H.; Tamayol, A.; Annabi, N.; Ochoa, M.; Mostafalu, P.; Akbari, M.; Nikkhah, M.; Rahimi, R.; Dokmeci, M. R.; Sonkusale, S.; Ziaie, B.; Khademhosseini, A. *Adv. Mater.* **2014**, *26*, 5823.
8. Ahmed, F. E.; Lalia, B. S.; Hashaikeh, R. *Desalination*. **2015**, *356*, 15.
9. Zhang, W.; Shi, Z.; Zhang, F.; Liu, X.; Jin, J.; Jiang, L. *Adv. Mater.* **2013**, *25*, 2071.
10. Liao, Y.; Wang, R.; Tian, M.; Changquan, Q.; Fane, A. G. *J. Membr. Sci.* **2013**, *425-426*, 30.
11. Zhang, R.; Liu, Y.; He, M.; Su, Y.; Zhao, X.; Elimelech, M.; Jiang, Z. *Chem. Soc. Rev.* **2016**, *45*, 5888.
12. Lee, J. W.; Jung, J.; Cho, Y. H.; Yadav, S. K.; Baek, K. Y.; Park, H. B.; Hong, S. M.; Koo, C. M. *ACS Appl. Mater. Interfaces*. **2014**, *6*, 14600.
13. Whitfield, M. J.; Bono, D.; Wei, L.; Van Vliet, K. J. *Corros. Sci.* **2014**, *88*, 481.
14. Li, K.; Whitfield, M. J.; Van Vliet, K. J. *Corros. Rev.* **2013**, *31*, 73.
15. Ouay, B. L.; Stellacci, F. *Nano Today*. **2015**, *10*, 339.
16. Liu, C.; Shen, J.; Yeung, K. W. K.; Tjong, S. C. *ACS Biomater. Sci. Eng.* **2017**, *3*, 471.
17. Yuan, J.; Geng, J.; Xing, Z.; Shen, J.; Kang, I. K.; Byun, H. *J. Appl. Polym. Sci.* **2010**, *116*, 668.
18. Hong, B.; Jung, H.; Byun, H. *J. Nanosci. Nanotechnol.* **2013**, *13*, 6269.
19. Shi, H.; Liu, F.; Xue, L. *J. Membr. Sci.* **2013**, *437*, 205.
20. Shi, H.; Liu, H.; Luan, S.; Shi, D.; Yan, S.; Liu, C.; Lic, R.; Yin, J. *RSC Adv.* **2016**, *6*, 19238.
21. Bui, H. T.; Chung, O. H.; Cruz, J. D.; Park, J. S. *Macromol. Res.* **2014**, *22*, 1288.
22. Wang, W.; Lu, Y.; Luo, M.; Zhao, Q.; Wang, Y.; Liu, Q.; Li, M.; Wang, D. *J. Appl. Polym. Sci.* **2016**, *133*, 44169.
23. Kolewe, K. W.; Dobosz, K. M.; Rieger, K. A.; Chang, C. C.; Emrick, T.; Schiffman, J. D. *ACS Appl. Mater. Interfaces*. **2016**, *8*, 27585.
24. Nishigochi, S.; Ishigami, T.; Maruyama, T.; Hao, Y.; Ohmukai, Y.; Iwasaki, Y.; Matsuyama, H. *Ind. Eng. Chem. Res.* **2014**, *53*, 2491.
25. Sun, Q.; Su, Y.; Ma, X.; Wang, Y.; Jiang, Z. *J. Membr. Sci.* **2006**, *285*, 299.
26. Jiang, S.; Cao, Z. *Adv. Mater.* **2010**, *22*, 920.
27. Mi, L.; Jiang, S. *Angew. Chem., Int. Ed.* **2014**, *53*, 1746.
28. Cheng, G.; Zhang, Z.; Chen, S.; Bryers, J. D.; Jiang, S. *Biomaterials*. **2007**, *28*, 4192.
29. Vasantha, V. A.; Rahim, S. Z.; Jayaraman, S.; Junyuan, G. H.; Puniredd, S. R.; Ramakrishna, S.; Teo, S. M.; Parthiban, A. *J. Mater. Chem. B*. **2016**, *4*, 2731.
30. Chang, Y.; Chang, W. J.; Shih, Y. J.; Wei, T. C.; Hsiue, G. H. *ACS Appl. Mater. Interfaces*. **2011**, *3*, 1228.
31. Zhai, G.; Toh, S. C.; Tan, W. L.; Kang, E. T.; Neoh, K. G. *Langmuir*. **2003**, *19*, 7030.
32. Chang, Y.; Ko, C. Y.; Shih, Y. J.; Quémener, D.; Deratani, A.; Wei, T. C.; Wang, D. M.; Lai, J. Y. *J. Membr. Sci.* **2009**, *345*, 160.
33. Wu, J.; Mather, P. *Polym. Rev.* **2009**, *49*, 25.
34. Zhou, H.; Yea, Q.; Xu, J. *Mater. Chem. Front.* **2017**, *1*, 212.
35. Piperno, S.; Lozzi, L.; Rastelli, R.; Passacantando, M.; Santucci, S. *Appl. Surf. Sci.* **2006**, *252*, 5583.
36. Ali, U.; Juhanni, K.; Karim, B. A.; Buang, N. A. *Polym. Rev.* **2015**, *55(4)*, 678.
37. Raut, H. K.; Dinachali, S. S.; He, A. Y.; Ganesh, V. A.; Saifullah, M. S. M.; Law, J.; Ramakrishna, S. *Energy Environ. Sci.* **2013**, *6*, 1929.
38. Luo, C. J.; Edirisinghe, M. *Macromolecules*. **2014**, *47*, 7930.
39. Zhang, C. L.; Yu, S. H. *Mater. Horiz.* **2016**, *3*, 266.
40. Ganesh, V. A.; Ranganath, A. S.; Baji, A.; Raut, H. K.; Sahay, R.; Ramakrishna, S. *Macromol. Mater. Eng.* **2017**, *302*, 1600387.
41. Kuo, W. H.; Wang, M. J.; Chien, H. W.; Wei, T. C.; Lee, C.; Tsai, W. B. *Biomacromolecules*. **2011**, *12*, 4348.
42. Chen, L.; Tan, L.; Liu, S.; Bai, L.; Wang, Y. *J. Biomater. Sci. Polym. Ed.* **2014**, *25*, 766.
43. Shokrollahi, F.; Zandi, M.; Shokrollahi, P.; Atai, M.; Ghafarzadeh, E.; Hanifeh, M. *Prog. Biomater.* **2017**, *6*, 147.
44. Chou, Y. N.; Wen, T. C.; Chang, Y. *Acta Biomater.* **2016**, *40*, 78.
45. Lutz, P. B.; Converse, E.; Cebe, P.; Asatekin, A. *ACS Appl. Mater. Interfaces*. **2017**, *9*, 20859.
46. Owens, D. K.; Wendt, R. C. *J. Appl. Polym. Sci.* **1969**, *13*, 1741.
47. Fowkes, F. M.; Kaczinski, M. B.; Dwight, D. W. *Langmuir*. **1991**, *7*, 2464.
48. Koch, B.; Jensen, L. E.; Nybroe, O. *J. Microbiol. Methods*. **2001**, *45*, 187.
49. Abrigo, M.; Kingshott, P.; McArthur, S. L. *ACS Appl. Mater. Interfaces*. **2015**, *7*, 7644.
50. Mandal, D.; Henkel, K.; Schmeißer, D. *Phys. Chem. Chem. Phys.* **2014**, *16*, 10403.
51. Zhang, W.; Li, G.; Lin, Y.; Wang, L.; Wu, S. *J. Biomater. Sci. Polym. Ed.* **2017**, *28*, 1935.
52. Zhang, X.; Zhang, Q.; Yan, T.; Jiang, Z.; Zhang, X.; Zuo, Y. Y. *Environ. Sci. Technol.* **2015**, *49*, 6164.
53. Ganesh, V. A.; Dinachali, S. S.; Nair, S.; Ramakrishna, S. *ACS Appl. Mater. Interfaces*. **2013**, *5*, 1527.
54. Ganesh, V. A.; Ranganath, A. S.; Baji, A.; Wong, H. C.; Raut, H. K.; Sahay, R.; Ramakrishna, S. *Macromol. Mater. Eng.* **2016**, *301*, 812.
55. Ganesh, V. A.; Nair, A. S.; Raut, H. K.; Tan, T. T.; He, C.; Ramakrishna, S.; Xu, J. *J. Mater. Chem.* **2012**, *22*, 18479.
56. Schlenoff, J. B. *Langmuir*. **2014**, *30*, 9625.
57. Khandwekar, A.; Patil, D.; Shouche, Y.; Doble, M. *J. Mater. Sci. Mater. Med.* **2010**, *21*, 635.
58. Kobayashi, M.; Terayama, Y.; Yamaguchi, H.; Terada, M.; Murakami, D.; Ishihara, K.; Takahara, A. *Langmuir*. **2012**, *28*, 7212.
59. Rieger, K. A.; Thyagarajan, R.; Hoen, M. E.; Yeung, H. F.; Forda, D. M.; Schiffman, J. D. *RSC Adv.* **2016**, *6*, 24438.

60. Kim, S. E.; Zhang, C.; Advincula, A. A.; Baer, E.; Pokorski, J. K. *ACS Appl. Mater. Interfaces*. **2016**, *8*, 8928.
61. Chang, Y.; Yandi, W.; Chen, W. Y.; Shih, Y. J.; Yang, C. C.; Chang, Y.; Ling, Q. D.; Higuchi, A. *Biomacromolecules*. **2010**, *11*, 1101.
62. Hsiao, S. W.; Venault, A.; Yang, H. S.; Chang, Y. *Colloids Surf. B Biointerfaces*. **2014**, *118*, 254.
63. Siddiqui, M. N.; Redhwi, H. H.; Vakalopoulou, E.; Tsagkalias, I.; Ioannidou, M. D.; Achilias, D. S. *Eur. Polym. J.* **2015**, *72*, 256.
64. Alsharaeh, E. H. *Materials*. **2016**, *9*, 458.
65. Singho, N. D.; Johan, M. R.; Che Lah, N. A. *Nanoscale Res. Lett.* **2014**, *9*, 42.
66. Afloria, M.; Simionescu, B.; Bordianu, I. E.; Sacarescu, L.; Varganicia, C. D.; Dorofteia, F.; Nicolescu, A.; Olaru, M. *Mater. Sci. Eng. B*. **2013**, *178*, 1339.
67. Sivashanmugan, K.; Liu, P. C.; Tsai, K. W.; Chou, Y. N.; Lin, C. H.; Chang, Y.; Wen, T. C. *Nanoscale*. **2017**, *9*, 2865.
68. Lalani, R.; Liu, L. *Biomacromolecules*. **2012**, *13*, 1853.
69. Xie, Y.; Tang, C.; Wang, Z.; Xu, Y.; Zhao, W.; Sun, S.; Zhao, C. *J. Mater. Chem. B*. **2017**, *5*, 7186.
70. Orooji, Y.; Liang, F.; Razmjou, A.; Liu, G.; Jin, W. *Sep. Purif. Technol.* **2018**, *205*, 273.
71. Shen, X.; Zhao, Y.; Chen, L. *Biofouling*. **2013**, *29*, 991.
72. Lee, J.; Yoon, J.; Kim, J. H.; Lee, T.; Byun, H. *J. Appl. Polym. Sci.* **2018**, *135*, 45858.
73. Goetz, L. A.; Jalvo, B.; Rosal, R.; Mathew, A. P. *J. Membr. Sci.* **2016**, *510*, 238.
74. Reeslev, M.; Nielsen, J. C.; Rogers, L. *J. ASTM Internl.* **2011**, *8*, 1.